Evolution of Surface Plasmon Supermodes in Metal-Clad Microwire and its Potential for Biosensing

N. S. Aminah, C. Themistos, Hendro, R. Hidayat, M. Djamal, and B. M. A. Rahman, *Fellow, IEEE*

***Abstract*— A finite element method (FEM) based on the vector H-field formulation in conjunction with perturbation techniques is used to study metal-clad microwire waveguides for bio-sensing applications. Sensors are designed to detect DNA hybridization through the change of the effective index and attenuation constant of the waveguide structure. The key parameters, such as effective index, loss coefficient, and spot-sizes are presented and potential sensor applications are discussed.**

***Index Terms*—Finite Element Method, Microwire, Surface Plasmon Resonance, Optical Sensing.**

I. Introduction

Surface plasmon mode is an electromagnetic wave that propagates along the interface between a metal and a dielectric [1]. Plasmonic mode based on surface plasmon resonance (SPR) are strongly confined at the metal-dielectric interface and such modes in a thin metal layer bound by two dielectrics are actually two even and odd-coupled plasmonic supermodes. The modal properties of these modes and their phase matching are very sensitive with any changes in the bounding layers and can be exploited in sensing applications.

Recently, micro- and nanowires have been explored as a means to detect DNA hybridization [2]. Among the different platforms, micro-and nanowires have been used as optical sensors because they have the advantage of high index contrast and low optical power losses [3-7]. However, the evolution of these plasmonic supermodes is quite complex, particularly when refractive indices of the bounding layers are different.

In this paper, we present a detailed numerical investigation of metal-clad microwires (MCMs) based SPR waveguide to detect DNA hybridization. Here, the complex propagation characteristics (both the phase and attenuation constants) of the coupled surface-plasmon modes and their evolution in a MCM are obtained by using the rigorous full-vectorial **H**-field based finite-element method (FEM).

II. MCM and Numerical Method

The MCM structure studied here is shown in Fig. 1. Such as MCM with a silica core can be fabricated from a silica fiber by controlled heating and drawing techniques [8,9]. Although, the full structure is shown here but only a quarter of the structure is simulated as available 2-fold symmetry is exploited. The metal used in this work is taken as silver. Biomolecular recognition elements immobilized on top of the metal layer. We assume that a sensing layer is initially functionalized by a 100 nm thick DNA monolayer on top of the biomolecular recognition elements layer of thickness, t_{cl} with a refractive index of n_{cl}. Here, it is assumed that the ssDNA molecules are changed to dsDNA in the presence of a target bio pathogen and as result its refractive index is changed from 1.456 to 1.53. This cladding layer with its refractive index n_{cl} and thickness t_{cl} can be adjusted to optimize the sensor design.

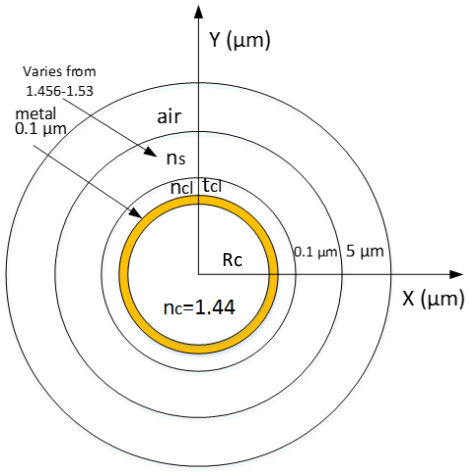

Fig. 1. Schematic of the MCM structure studied.

N. S. Aminah is with the Theoretical High Energy Physics and Instrumentation, Institut Teknologi Bandung, Jl. Ganesha no. 10, Bandung 40132, Indonesia (e-mail: nina@fi.itb.ac.id).

C. Themistos is with the Department of Electrical Engineering, Frederick University, 7, Y. Frederickou Str. Pallouriotisa, Nicosia 1036, Cyprus (e-mail: eng.tc@frederick.ac.cy).

Hendro is with the Theoretical High Energy Physics and Instrumentation, Institut Teknologi Bandung, Jl. Ganesha no. 10, Bandung 40132, Indonesia (e-mail: hendro@fi.itb.ac.id).

R. Hidayat is with the Physics of Magnetism and Photonics, Institut Teknologi Bandung, Jl. Ganesha no. 10, Bandung 40132, Indonesia (e-mail: rahmat@fi.itb.ac.id).

M. Djamal is with the Theoretical High Energy Physics and Instrumentation, Institut Teknologi Bandung, Jl. Ganesha no. 10, Bandung 40132, Indonesia (e-mail: mitra@fi.itb.ac.id).

B. M. A. Rahman is with the School of Mathematics, Computer Science and Engineering, City, University of London, Northampton Square, London, EC1V 0HB, UK (e-mail: B.M.A.Rahman@city.ac.uk).

A single dielectric/metal (D/M) interface can support a SPM and two such modes in two adjacent interfaces (either D-M-D or M-D-M slab) couple to form even and odd supermodes. Modes in such a three-layers planar waveguide have been extensively studied [10] but such mode in MCM has not been rigorously studied. Here, a MCM with silica core (SiO_2) and radius R_c is considered. The metal used in this work is taken as silver with its refractive index, n_s = 0.14447 + j 11.366 at the operating wavelength λ = 1.55 μm [11]. Refractive index of silica is taken as n_{SiO_2} =1.44, at the same operating wavelength.

An in-house rigorous full-vectorial **H**-field FEM in conjunction with the perturbation techniques [12] is used to obtain the modal solutions of waveguides with complex refractive indices associated with the metal layers. Perturbation is a powerful numerical technique [13,14], however only applicable when the modal loss or gain is small. Although a general-purpose FEM solver can find the complex modes without the limit of a perturbation approach, however the computational cost is higher than a perturbation based FEM code, as used here.

Here, using more efficient mesh generation code conforming polar coordinates has been used to incorporate a fine mesh inside a very thin metal layer. Initially, optimizations of design parameters, such as core radius, metal thickness, and cladding thickness are carried out. Subsequently the effective index, loss coefficient, and spot-sizes of the MCM have been calculated to study the evolution of coupled plasmonic supermodes.

Although this structure has a circular symmetry, but this is not exploited in the simulations. In fact, for such a waveguide with circular symmetry, as the modal field may not always be azimuthally invariant, so this should not be imposed as discussed later on. On the other hand, in this work the available two-fold mirror symmetry has been explored to increase the computational efficiency. So only a quarter of the MCM is simulated as shown as an inset in Fig. 2 and this represented by nearly a million first-order triangles with very fine mesh density inside the thin metal layer. The polar coordinate discretization used here which matches more accurately to the circular cross sectional area of the waveguide which allows very fine mesh inside the thin metal layer.

III. Result

Figure 2 shows variations of the effective indices, n_e, with the metal thickness, *t*, for different values of core radius, R_c. The effective index is calculated as n_{eff}= β/k_o, where β is the propagation constant and k_o is the free-space wavenumber. Initially a large cladding thickness with its index same as that of the core is considered to study evolution of supermodes. The coupled mode in identical bounded media remains symmetric or asymmetric for a planar guide (R = ∞) as the isolated modes are always phase matched. However, in this case as the isolated modes at each M/D interface are not phase matched (as their bending radii are different) so the coupled supermodes become non-symmetric. These two supermodes are examined, the first one corresponding to the 'odd-like' supermode (M_o) and the second to 'even-like' supermode (M_e). Both these supermodes have higher effective indices than the cladding refractive index, $n_{cl} = n_{SiO_2}$. The effective index (n_e) of the even-like supermode (M_e) decreases and approaches the cladding refractive index value as the metal thickness decreases. But for the odd-like supermode (M_o), as the film thickness reduces, its effective index increases. When the metal film thickness becomes large, these two D/M SPMs become separated and have similar effective indices. For the odd-like supermodes shown by two upper lines, they are nearly anti-symmetric when the metal thickness is small. However, when the metal thickness, *t* is increased to 100 nm, the non-symmetry becomes more pronounced (as weakly coupled). As in that case, this mode is predominantly confined at the metal-cladding interface so not affected by the diameter of the microfiber. On the other hand, as metal thickness is increased to 100 nm, similarly the even-like nearly symmetric mode also becomes non-symmetric and this mode is mostly confined at the core-metal interface. As this mode is confined inside the microfiber core, so its effective index depends on the core diameter and this difference can be noted when core radius is reduced from 10 μm to 5μm, shown by dotted red and solid blue lines, respectively. When R_c increases, both these modal effective indices converge to the effective index value of the SPM of a single D/M interface.

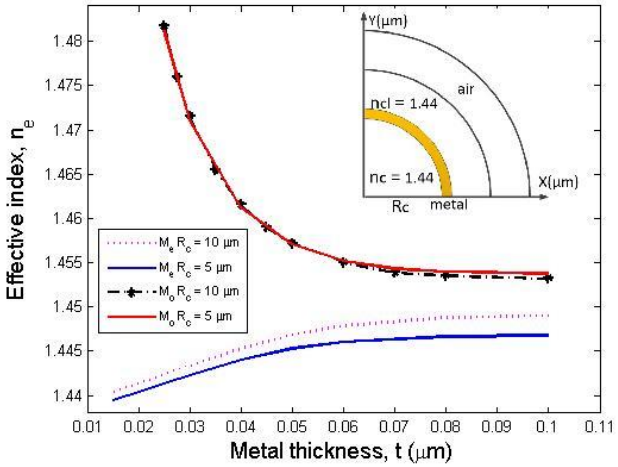

Fig. 2. Variation of the effective indices for surface plasmon resonance structure, a quarter of the MCM is shown as an inset.

Next, H_y field contour profile of the H_{11}^y even-like supermode is shown in Fig. 3, when the core radius R_c = 10 μm and metal thickness, *t* = 0.04 μm. For this mode, when the electric boundary wall condition, $\mathbf{n} \cdot \mathbf{H} = 0$ is implemented at the right side metal walls, this allows the H_y field to be non-zero at the D/M interfaces, and forms a SPM (with dominant H_y field). However, the same dominant H_y field is zero at the top D/M interface, to satisfy the electric wall boundary condition, and thus no SPM (with dominant H_y field) can form along that interface. This enforcement of the boundary condition destroys the circular symmetry of the modes, which can be clearly observed in Fig. 3. So in such a case the available circular symmetry (of the structure) should not be imposed. The even-like supermode shown is no longer symmetric (along the x-axis) as expected in a uniform planar

guide (which has two modes, perfectly symmetric and anti-symmetric) even tough in this case bounding dielectrics were identical $n_c = n_{cl} = 1.44$. However, for a curve metal layer the modes at two D/M interfaces are not exactly phase matched. In this case, the even-like supermode is more concentrated in the core region, which has a smaller radius than the cladding. When the metal thickness, *t* is reduced, due to stronger coupling the symmetry is increased and progressively more field is confined in the cladding region. It can be observed that peak field (rather two peaks) follows the two metal/SiO_2 curved interfaces with a small plasmonic dip (as for an even-like mode) inside the metal layer shown by a red arrow. Similar SPM with dominant H_x field will also form at the upper and lower horizontal interfaces, but not shown here. These two SPMs are degenerate with the same propagation constants, but as we have used the 2-fold symmetry, we were able to isolate them by using different boundary conditions at the vertical and horizontal axes.

Variation of H_y field along the x-axis is also shown as an inset. From the inset it can be observed that the optical field profile along x-axis has maximum field intensity at the two D/M interfaces at the radial distance of ~ 10 μm and decays in the core and cladding away from the D/M interfaces. A slightly larger peak at the core/metal interface can be observed. A small dip for this even-like supermode inside this thin metal layer is shown by a blue arrow.

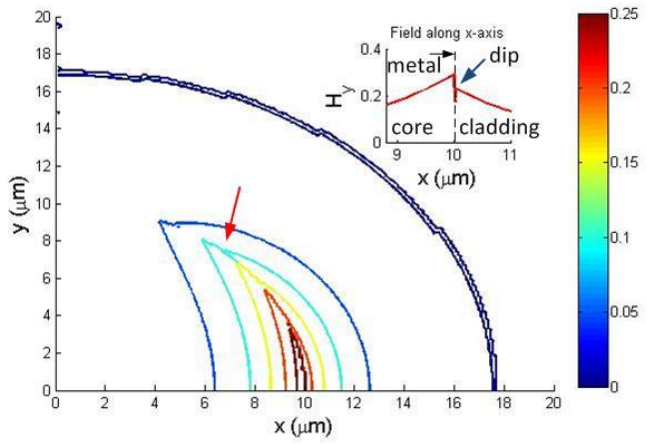

Fig. 3. H_y field profile for the even-like supermode when R_c = 10 μm and t = 0.04 μm, field profile near the metal layer is shown as an inset.

In this work, modal losses of these modes are calculated by the perturbation approach [17]. Loss arises from the light confinement inside the metal layer with a complex refractive index. Loss curves shown in Fig. 4 have similar shapes as the effective index curves, as discussed previously for a simple plasmonic slab waveguide [19]. For the odd-like supermodes, shown by two upper lines in Fig. 4, as *t* is reduced, modes get more confined in the metal layer and spread less in the bounding dielectric layers (considered here as loss-less). For a thinner metal layer, more power is confined in the lossy metal layer and as a result modal loss is also increased. On the other hand, for the even-like supermode, shown by two lower lines, as *t* is reduced, these modes approach their cutoff, field extends more in the bounding dielectric layers. As in this case power confinement in metal layer is reduced, which progressively lower the modal loss. It can be noted that as the even-like supermode can propagate a longer distance so also known as a 'long-range' mode and similarly the odd-like first supermode with higher loss known as a 'short-range' mode. Here, we have ignored the loss from the other materials or from surface scattering, but if needed they can also be included. The H_y field profiles of the odd-like supermode along the *x*-axis are shown for t = 40 nm and 100 nm by two upper insets, A and B, respectively. It can be observed that, at the larger *t*, the upper-right inset B shows that the asymmetry gets more pronounced due to weaker mode coupling and confines less power in the core region. The lower-left inset, C shows the H_y field profile of the even-like supermode.

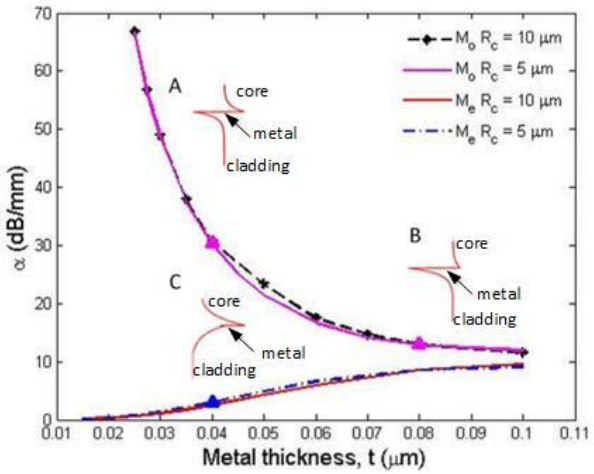

Fig. 4. Variation of loss coefficient versus metal thickness for two core radius, H_y field profiles are shown as insets.

The metal thickness influences field variation inside the bounding dielectric layers, which also change the spot-size of the modes. Field confinement can be quantitatively described by its mode-size or spot-size. It can be defined as a distance or as an area. In this work, because of the asymmetry of the mode shape, the spot-size is taken as the distance along the x-axis where the modal field is equal to the 1/*e* times of the maximum value at the interface (see inset in Fig.5). Since field decay in the two bounding interfaces are different, σ_+ and σ_- are taken as spot-sizes at the right interface (cladding region) and the left interface (in the core region), respectively. Variations of the spot-sizes of the even-like supermode for core radius, R_c = 5 μm and 10 μm are shown in Fig. 5. The spot-size, σ, increases as the metal thickness is reduced as the mode approaches its cutoff. The σ_+ values are similar for both R_c = 5 μm and 10 μm, shown by red chained and black solid lines, respectively. The σ_- values are larger as field decays slowly in the inner core layer. The σ_- is larger when R_c is lower as field decays more slowly. It should be noted that for the odd-like supermode, its spot-size decreases as the metal thickness is reduced, but not shown here.

However, for a sensor design, access to modal field is needed. A thicker cladding thickness will inhibit sensing material to influence the modal properties. Therefore, leaving too much of the cladding after the metal layer weakens the interaction between the optical mode and sensing media and thus evanescent sensing field can be exposed by partial

removal of the cladding. For this reason next, the effect of finite cladding thickness on the supermodes is studied.

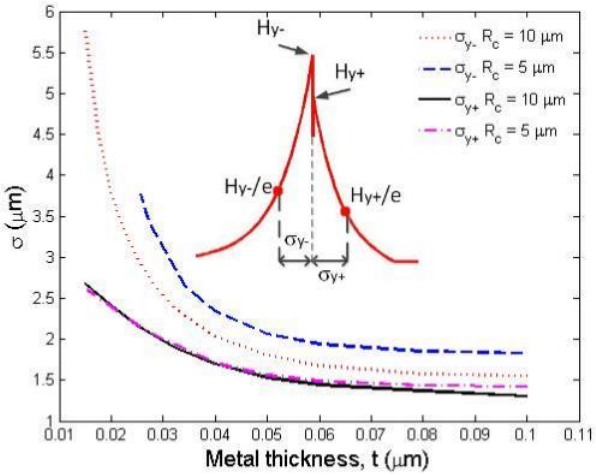

Fig. 5. Variations of spot-sizes of the H_y field for the H_{11}^y mode with the metal thickness, when core radius $R_c = 10\mu m$, H_y field profile and the spot size definitions are shown as an inset.

Variations of the effective indices for the M_o and M_e supermodes with the cladding thickness are shown in Fig. 6 by a red dashed and a solid lines, respectively, for $n_{cl} = 1.44$. When $n_c = n_{cl} = 1.44$, refractive index values of both the bounding sides were identical, however in Fig. 5 it was shown that modes were not symmetrical as the metal interfaces were curved. The M_o supermode profile for a thicker cladding, shown as upper-right inset, B showing a more asymmetric profile and confining more at the metal-cladding interface. As the cladding thickness is reduced, the effective index of the odd-like supermode also reduces as shown by a dashed red line and for very low cladding thickness this mode transforms to a SPM at the core-metal interface. On the other hand, the even-like supermode, shown by the red solid line initially reduces slowly when mode is more confined at the core-metal interface shown as Inset C. When cladding thickness is very small, its effective index reduces rapidly and this mode transforms to a SPM mainly confining at the clad-metal interface. It can be noted that when cladding thickness is about 1.875 μm, the difference between these two effective indices is the smallest. In this case, two isolated SPM at the upper and lower M/D interfaces are phase matched. As a result, nearly perfect odd and even supermodes are formed and these two SPMs are shown by two left insets, A and D, respectively.

The M_e curve (solid line) on the right-side of the phase matching point and the M_o curve on the left of the phase matching point (dashed line) are related to the SPM mode at the core-metal interface. This mode is not much influenced by the cladding thickness so almost horizontal. Similarly the dashed curve (M_o mode) right of the phase matching point and the lower part of the solid curve (M_e mode) left of the phase matching point, together represent the SPM at the metal-cladding interface. Effective index of this mode strongly depends on the cladding thickness and reduces very fast, when air comes close to the metal interface for a very small cladding thickness. These two effective index curves never intersect but form an anti-crossing point when the two isolated modes are phase matched. At that situation rapid mode transformation is possible and can be exploited for a sensor design.

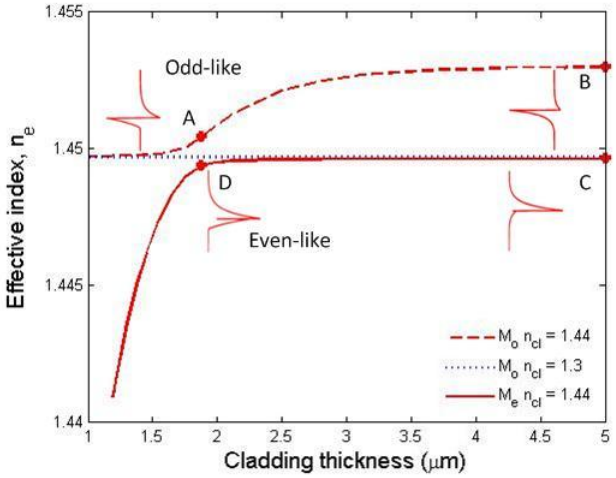

Fig. 6. Effective index at a fixed metal thickness, t = 0.1μm for different cladding's refractive index and thickness, for core radius, R_c = 10 μm.

The effective index of the SPM mode at core/metal interface when $n_{cl} = 1.3$ is also shown by a black dotted line as a reference. In this case, SPM mode at the metal/cladding interface does not couple with the SPM at the core/metal interface, as their effective indices are very different and this mode is not shown here.

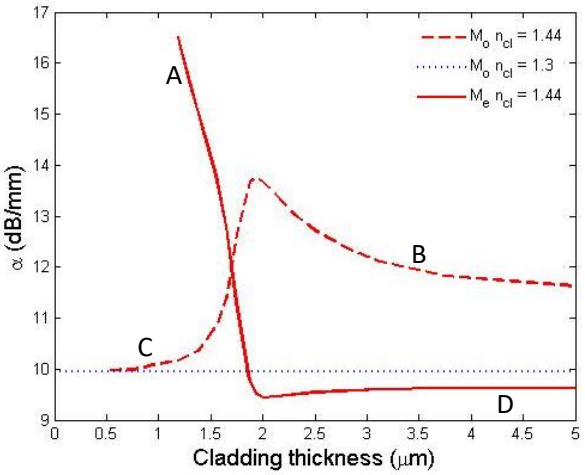

Fig. 7. Loss calculation at a metal thickness, t = 0.1μm for different cladding's refractive index and thickness, for core radius, R_c = 10 μm, R_c = 10 μm, transition points are identified by insets.

Next, attenuation constants for these modes are also calculated and shown in Fig. 7. Here, the red solid line represents the attenuation curve for the even-like supermode and the red dashed line represents the odd-like supermode, when $n_c = n_{cl}$. As the cladding thickness decreases, attenuation constants for the odd-like supermode increases slowly at first, then more rapidly, but after reaching a peak value drops to a very low value. However, the attenuation constant of the even-like supermode reduces slightly as the cladding thickness reduces, however, near $t_{cl} \sim 1.875$ μm rapidly increases.

For cladding refractive index value lower than core refractive index, n_{cl} = 1.3, effective index and attenuation constant for the odd-like the SPM mode at the core/metal interface mode remain constant and the attenuation curve for this mode is also shown by a black dotted line for a reference. The right part of the solid line (M_e), although part of an even-like supermode, but shows attenuation value of a mode which is more confined in core/metal interface. Similarly the left part of the dashed line, attenuation constant of the odd-like supermode, M_o, but this part also represents the SPM which is predominantly confines at the core/metal interface. These attenuation values are similar to that of the isolated SPM at the core/metal interface, shown in this figure by a dashed line for highly asymmetrical cladding with n_{cl} = 1.3. Similarly the right section of the dashed line (of the odd-like supermode) and left part of the solid line (of the even-like supermode), represents a SPM mainly confined at the metal/cladding interface with a higher loss value. As cladding thickness is reduced, the modal loss of this SPM is strongly influenced by the presence of air just outside the thin cladding layer. In the transient region, when SPMs at both the interfaces are phase matched the loss values go through a rapid transition, which can be exploited for optical sensing.

As the effective index of the SPM at the outer boundary metal/cladding interface will be smaller when $n_{cl} < n_c$ this mode will not interact with the SPM at the core/metal interface when cladding thickness is reduced. On the other hand, the effective index of the SPM at the metal/cladding interface will increase for a higher n_{cl} value, and when its cladding thickness is reduced, this effective index value is expected to reduce and cross the effective index value of the SPM at the core/metal interface and together they form coupled supermodes. For a slightly higher n_{cl} value, slope of this line can be higher and this interactions will also be sharper.

For cladding refractive index value slightly higher than core refractive index, n_{cl} = 1.45, variation of the effective indices for the even and odd-like supermodes are shown in Fig. 8 by a solid and a dashed blue lines, respectively. The effective index variations for n_{cl} = 1.44, which was shown earlier in Fig. 6, are also shown here by red lines for comparison. Higher cladding refractive index value gave higher effective index value and sharper slope for the odd-like supermode. For even-like supermode, its effective index value is similar as the earlier case with n_{cl} = 1.44 when the cladding thickness is large, but subsequently decreases as the cladding thickness reduces. As n_{cl} increase from 1.44 to 1.45 slope of this curve increases near phase matching point. Sharper slope yields a smaller effective index difference. This resonant point is most sensitive with any perturbation in the presence of a sensing media and this can be exploited.

Variations of the attenuation constants for n_{cl} =1.45 are shown in Fig.9 by blue curves. In this case the solid line represents the attenuation curve for the even-like 2nd supermode and the dashed curve represents the first odd-like supermode, for the case $n_{cl} > n_c$. The loss values for n_{cl} = 1.44, earlier shown in Fig.7, are also shown here by red lines for comparison. As the cladding thickness decreases, attenuation constants for odd-like mode increases slowly at first, then more rapidly, reaches a peak value and then drops to the same value as even-like supermode and this occurs at the phase-matching point when the attenuation constant of even-like supermode increased significantly. The higher n_{cl} value gives faster attenuation transient and the phase matching point shifts to a smaller thickness.

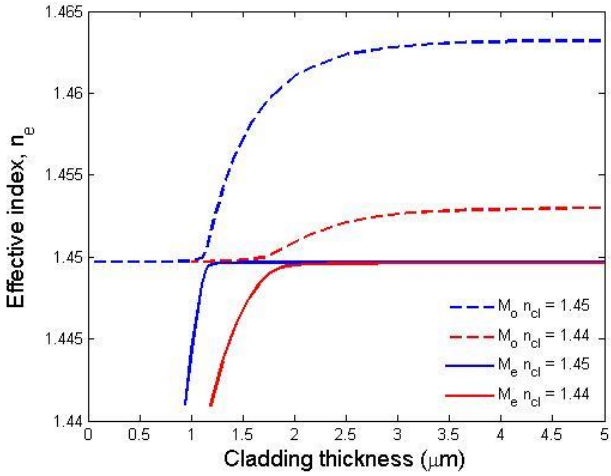

Fig. 8. Effective index at a metal thickness, t = 0.1μm for different cladding's refractive index and thickness, for core radius, R_c = 10 μm.

Next, possibility of exploiting this rapid transition for developing biosensors is studied. Here the core radius is kept fixed at R_c = 10 μm and the metal thickness, t_s = 0.1 μm. We assume that a sensing layer is initially functionalized by a 100 nm thick DNA monolayer on top of the cladding layer of thickness, t_{cl} with a refractive index of n_{cl}. When a detection event happens, the complementary target single strand DNA (ssDNA) would hybridize to double stranded DNA (dsDNA) and its refractive index value changes. We will study the effect of cladding thickness in the presence of ssDNA and dsDNA. The ssDNA and dsDNA refractive indices are taken as 1.456 and 1.53 [15-18], respectively.

The rapid change in the loss values due to the presence of the sensing biomaterials can be used for sensing applications. The differential losses between the modes, due to the change of the ssDNA to dsDNA, are shown in Fig. 10. It should be noted that, with proper design when the SPMs at two interfaces are phase matched any slight change in waveguide parameters will alter modal properties significantly. In such a case, the rapid change in the loss values due to the presence of a target biomaterial can be exploited for sensing applications. A small change in the sensing index from 1.456 to 1.53 makes a significant change in the modal loss values. The differential losses due to the change of the ssDNA to dsDNA, for different modes are shown in Fig. 10. Here, only the differences between these two loss values are shown by solid and dotted lines, for the odd and even-like supermodes, respectively. Here, we have also considered two different values of the cladding index, n_{cl} = 1.459 and 1.463, and shown here by using blue and red lines, respectively. The n_{cl} values considered here are slightly higher than those considered in Fig. 9, as the transients were identified to be even faster.

It can be observed from Fig. 10 that as the cladding thickness is increased, initially the differential loss increases, reaches a maximum value, $\Delta\alpha_{max}$, and then reduces. This

maximum location for a given n_{cl} is at the same value of t_{cl}, when the supermodes are phase matched. It is shown here that

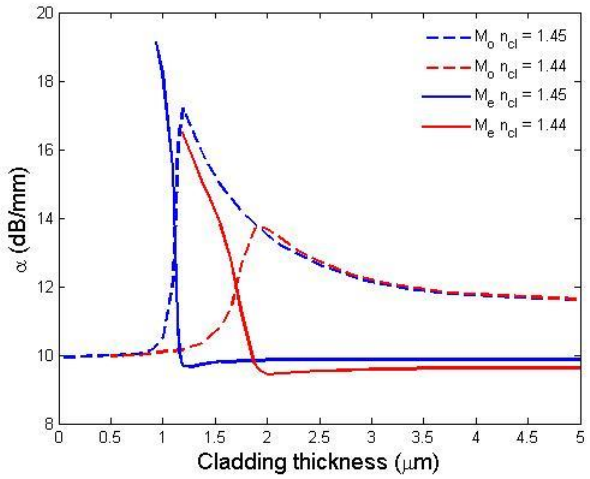

Fig. 9. Loss calculation at a metal thickness, t = 0.1μm for different cladding's refractive index and thickness, for core radius, R_c = 10 μm.

for n_{cl} = 1.459, the $\Delta\alpha_{max}$ = 4.42 dB/mm. So, we only need a 2.23 mm long section to achieve a 10 dB extinction coefficient. However, as the lower loss was 11.802 dB/mm, unfortunately the Insertion Loss will also be 26.32 dB. However, when, n_{cl} is increased to 1.463, the differential loss increases to 5.51 dB/mm, shown by red lines. This would shortens the device length to 1.81 mm and the IL will also reduce to 21.48 dB, albeit only slightly.

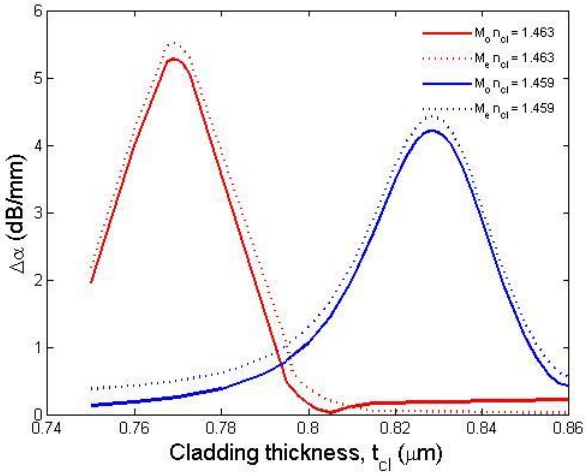

Fig. 10. Variations of the loss calculation difference with the change in the cladding thickness for two different cladding index values, 1.459 and 1.463. In both cases changes are due to target index changing from 1.456 to 1.63.

Alternatively, in order to detect the DNA hybridization, this MCM can also be incorporated in a Mach-Zehnder Interferometer (MZI) system. By introducing the sensing waveguide in one arm of the MZI, the relative phase shift $(\Delta\phi)$ can be obtained from the change in the effective index, Δn_e, as

$$(\Delta\phi) = \Delta n_e \times \frac{2\pi}{\lambda} \times L \qquad (1)$$

The destructive interference or the minimum interference signal occurs when the phase difference is equal to π.

Here, we also show the difference between the effective indices due to change in n_s from 1.456 to 1.53 when ssDNA transforms to dsDNA. The even and odd-like supermodes are shown by solid and dashed lines, respectively. Similarly the changes for n_{cl} = 1.459 and 1.463 are shown by blue and red lines respectively. The maximum Δn_e values can also be observed for the odd-like supermodes at the transient points. For n_{cl} = 1.459, this value was 0.008 but for higher cladding index value, n_{cl} = 1.463, this value is increased to 0.0012, when the cladding thickness is 0.8 μm. The length required for the sensing arm would be 0.65 mm, yielding a reasonably compact device. However, this would also introduce 7 dB loss to the sensing branch signal and that could yield a significant cross-talk as the signals will not be cancelled, even they have a π phase shift. However, it may be possible to introduce additional loss in the control branch, to improve the performance.

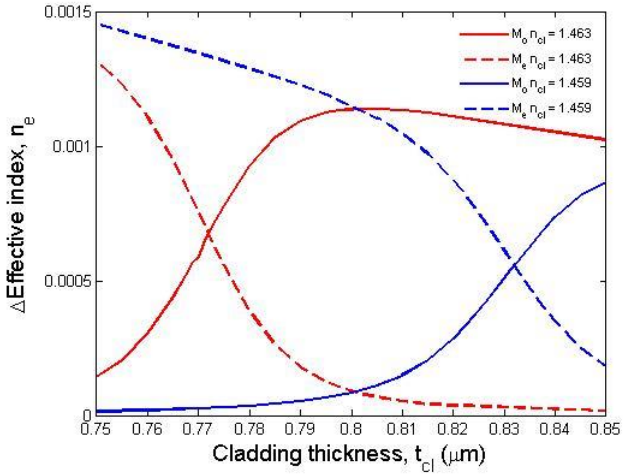

Fig. 11. Variations of the effective index difference with the change in refractive index of sensing material.

However, we have noticed another case, when the cladding thickness is reduced further and shown in Fig. 12. Variations of the effective index and effective index difference with or without the presence of sensing target with the cladding thickness are shown. The effective index values for the even-like supermodes (M_o), are shown by black dashed and dotted lines when n_s = 1.456 (ssDNA) and 1.53 (dsDNA), respectively. It can be observed that there is not much difference between these two curves, as this mode is primarily confined at the core/metal interface. Their difference is shown by the blue solid line. This shows a small peak at the right-end, which represents the same peak shown by the solid blue line in Fig.11 (where a magnified scale was used). However, in this case, the odd-like supermode (M_e) shows a significant difference when cladding value is much smaller. The effective index values before (with ssDNA) and after (with dsDNA) are shown by solid and dashed-dotted black lines. Their difference is shown by a blue dotted line. This shows a large index difference of 0.015 can be obtained when t_{cl} = 0.016 μm. In this case most of the power is confined in this odd-like supermode confining predominantly at the metal-cladding interface. This would yield a significantly shorter, only 48 μm

long sensing section and associated modal loss is only 0.5 dB, and can provide a more promising design.

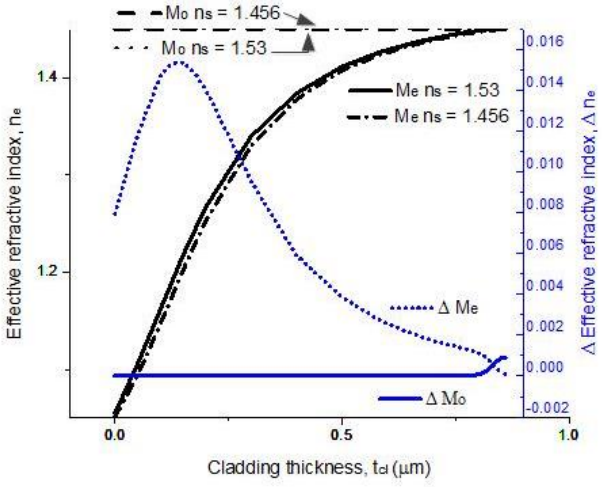

Fig. 12. Effective index (ne) and effective index difference (Δn_e) as a function of cladding thickness, t_{cl}

The relative phase change due to the presence of a sensing material can be identified by a MZI-based design [19]. Here, the proposed MZI-based biosensor system formed by using two uniform metal-clad microwires, are shown in Fig. 13, where one arm is used as a reference arm and the other as the sensing arm. A probe light can be launched through the microwire propagates along the Y-branch, which divides equally between the sensing and the reference arms and subsequently recombines. The phase shift caused by the index change due to the specimen placed in the sensing arm has been numerically calculated. It is shown here that a compact 48 μm long sensing arm can be adequate with insertion loss only 0.5 dB.

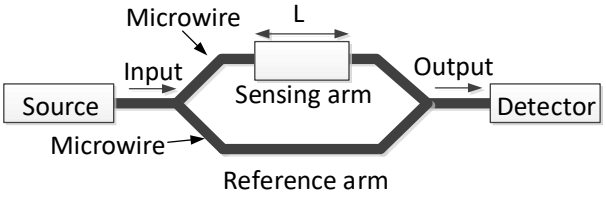

Fig. 13. Scheme of integrated Mach-Zehnder Interferometer

IV. Conclusion

Evolutions of supermodes at the two M/D interfaces and their phase matching are studied here. The resulting field profiles, effective index, and attenuation constants characteristics of the SPMs for the MCMs structure are presented by using a full-vectorial **H**-field based FEM in conjunction with the perturbation technique. The sensing materials considered in the present work are ssDNA and dsDNA in the DNA hybridization process. The optimum dimensions for the metal-clad microwires in order to achieve maximum effective index difference, or loss differences were found to be at the phase matching point; however, the loss values were significantly higher. On the other hand, by bringing the cladding thickness to only 0.15 μm, a more compact 48 μm long sensing arm with only 0.5 dB loss can be achieved. The prospects of suitable biosensors using MCM is discussed here. However, a system level analyses now need to be undertaken by considering excitations of various modes at the microwire and MCM junctions, including their performances with fabrication tolerances and wavelength variations.

Acknowledgment

This work was supported by City, University of London. The authors thank Erasmus Mundus Intact for research funding.

References

[1] H. Raether, “Surface plasmon oscillations and their applications. Physics of thin films,” Florida, USA: A. Press, 1977, pp. 145-262.

[2] K. Ramanathan, M.A. Bangar, M. Yun, W. Chen, N.V. Myung, and A. Mulchandani, “Bioaffinity sensing using biologically functionalized conducting-polymer nanowire,” *J. Am. Chem. Soc.*, vol. 127, no. 2, pp. 496–497, Jan. 2005.

[3] F. Dell’Olio and V.M. Passaro, “Optical sensing by optimized silicon slot waveguides,” *Opt. Express*, vol. 15, no. 8, pp. 4977–4993, Apr. 2007.

[4] D.J. Sirbuly, A. Tao, M. Law, R. Fan, and P. Yang, “Multifunctional nanowire evanescent wave optical sensors,” *Adv. Mater.*, vol. 19, no. 1, pp. 61–66 Dec. 2006.

[5] B. MacCraith, V. Ruddy, C. Potter, B. O’Kelly, and J. McGilp, “Optical waveguide sensor using evanescent wave excitation of fluorescent dye in sol-gel glass,” *Electron. Lett.*, vol. 27, no. 14, pp. 1247–1248, 1991.

[6] J. Lou, L. Tong, and Z. Ye, “Modeling of silica nanowires for optical sensing,” *Opt. Express*, vol. 13, no. 6, pp. 2135–2140, March 2005.

[7] J. Wang and D. Dai,” Highly sensitive Si nanowire-based optical sensor using a Mach–Zehnder interferometer coupled microring,” *Opt. Lett.*, vol. 35, no. 24, pp. 4229–4231, Dec. 2010.

[8] G. Brambilla, et al, “Ultra-low-loss optical fiber nanotaper,” *Optics Express*, vol. 12, no. 10, pp.2258-2263, 2004.

[9] G Brambilla, et al, “Optical fiber nanowires and microwires: fabrication and applications,” *Advances in Optics and Photonics*, vol. 1, no. 1, pp.107-161, Jan. 2009.

[10] Yi-Fan Li and John W. Y. Lit, "General formulas for the guiding properties of a multilayer slab waveguide," *J. Opt. Soc. Am. A*, vol. 4, no. 4, pp. 671-677, Apr. 1987.

[11] P. B. Johnson and R. W. Christy, “Optical constants of the noble metals,” *Phys. Rev. B*, vol. 6, no. 12, pp. 4370–4379, Dec. 1972.

[12] C. Thermistos, B. M. A. Rahman and K. T. V. Grattan, “Finite-element analysis of surface-plasmon modes for lossy optical waveguides by the use of perturbation techniques”, *Appl. Opt*. vol. 34, no. 33, pp. 7695-7701, Nov. 1995.

[13] V. Krishnamurthy and B. Klein, "Theoretical investigation of metal cladding for nanowire and cylindrical micropost lasers." *IEEE Journal of Quantum Electronics*, vol. 44, no. 1, pp.67-74, Jan. 2008.

[14] C. Themistos, B. M. A. Rahman, A. Hadjicharalambous, and K. T. V. Grattan, “Loss/gain characterization of optical waveguides”, *J. Lightwave Technol*, vol. 13, no. 8, pp.1760-1765, Aug. 1995.

[15] S. Elhadj, G. Singh and R. F. Saraf, “Optical properties of an immobalised DNA monolayer from 255 nm to 700 nm”, *Langmuir*, vol. 20, no. 13, pp. 5539-5543, May 2004.

[16] C. Viphavakit, M. Komodromos, C. Themistos, W. S. Mohammed, K. Kalli, and B. M.A. Rahman, “Optimization of a horizontal slot waveguide biosensor to detect DNA hybridization,” *Appl. Opt.*, vol. 54, no. 15, pp. 4881-4888, 2015.

[17] S. Ghosh and B. M. A. Rahman, “An Innovative Straight Resonator Incorporating a Vertical Slot as an Efficient Bio-Chemical Sensor,” *IEEE Journal of Selected Topics in Quantum Electronics*, vol. 23, no. 2, pp. 132-139, March 2017.

[18] C. Pan and B. M. A. Rahman, “High-Sensitivity Polarization-Independent Biochemical Sensor Based on Silicon-on-Insulator Cross-Slot Waveguide”, *IEEE Journal of Selected Topics in Quantum Electronics*, vol. 23, no. 2, pp. 64-71, March 2017.

[19] B. J. Luff, J. S. Wilkinson, J. Piehler, U. Hollenbach, J. Ingenhoff, and N. Fabricius, “Integrated optical Mach–Zehnder biosensor”, *J. Lightwave Technol*, Vol. 16, no.4, pp. 583-592, April 1998.

Nina Siti Aminah was born in Bogor, Indonesia. She received her B.Eng in Electronics from National Institute of Technology, Indonesia and B.S and M.S degree in Physics from Bandung Institute of technology, Indonesia. She is currently pursuing Ph.D degree at the Theoretical High Energy Physics and Instrumentation, Bandung Institute of Technology.
Currently she is working as a lecturer at Theoretical High Energy Physics and Instrumentation, Bandung Institute of Technology.

C. Themistos received the B.Eng. and Ph.D. degrees in electrical engineering from the City University, London, U.K., in 1992 and 1998, respectively. His Ph.D. degree involved the development of a finite-element-method-based approach, in conjunction with the perturbation technique, for the analysis of loss and gain in optical waveguides.
His research interests involve the application of finite-element-based approaches for the characterization of photonic devices, such as multimode interference-based designs, optical modulators, and the analysis of surface plasmon modes in optical waveguides at optical and terahertz frequencies. Since 2000, he has been with the Photonic Devices Modelling group at the City University, and the Frederick Research Centre, Cyprus, and he has been involved in projects funded by the industry, the Research Promotion Foundation, Cyprus, and the Royal Society, U.K.

Hendro received the B.S. and Ph.D. degrees in physics from Bandung Institute of Technology, Bandung, Indonesia, in 1982 and 2010, respectively. In 1983, he joined Bandung Institute of Technology, Bandung, Indonesia, as a Lecturer.

R. Hidayat received the B.S. degrees in physics from Bandung Institute of Technology, Bandung, Indonesia, in 1993. He received his Master and Ph.D. degree from Osaka University, Japan in 1998 and 2001 respectively. In 1994, he joined Bandung Institute of Technology, Bandung, Indonesia, as a Lecturer.

M. Djamal received the B.S. degrees in physics from Bandung Institute of Technology, Indonesia and Ph.D. degree from Universitat der Bundeswehr Munchen, Germany in 1984 and 1992 respectively. In 1984, he joined Bandung Institute of Technology, Bandung, Indonesia, as a Lecturer, where he is now a Professor, and leads the research group on theoretical high energy physics and instrumentation.

B. M. A. Rahman (S'80 - M'83 - SM'94 - F'2016) received his B.Sc Eng. And M.Sc. Eng. Degrees (with distinctions) in Electrical Engineering from the Bangladesh University of Engineering and Technology (BUET), Dhaka, Bangladesh, in 1976 and 1979, respectively, and received two gold medals for being the best undergraduate and graduate students of the university in 1976 and 1979, respectively. In 1979, he received a Commonwealth Scholarship and in 1982 obtained a Ph.D degree in Electronics from University College London, London, U.K.
From 1976 to 1979, he was a Lecturer in the Department of Electrical Engineering, BUET. In 1982, he was a Postdoctoral Research Fellow at University College London. In 1988, he joined City, University of London, London, U.K., as a Lecturer, where he became a full Professor in 2000, and leads the research group on photonics modelling, specialized in the use of rigorous and full-vectorial numerical approaches to design, analyse, and optimize a wide range of photonic devices, such as spot-size converters, high-speed optical modulators, compact bend designs, power splitters, polarization splitters, polarization rotators, polarization controllers, THz devices, etc. He is the author or co-author of more than 500 journal and conference papers, and his journal papers have been cited more than 4200
times. He is a Fellow of the IEEE, Optical Society of America (OSA) and SPIE. He is a Chartered Engineer, U.K.